

Magnetic Rossby waves in the solar tachocline and Rieger-type periodicities

Teimuraz V. Zaqarashvili^{1,3}, Marc Carbonell², Ramón Oliver³, and José Luis Ballester³

Received _____; accepted _____

¹Abastumani Astrophysical Observatory at Faculty of Physics and Mathematics, Ilya Chavchavadze State University, Chavchavadze Ave 32, 0179 Tbilisi, Georgia. Email: temury.zaqarashvili@iliauni.edu.ge

²Departament de Matemàtiques i Informàtica.
Universitat de les Illes Balears,
E-07122 Palma de Mallorca, Spain. Email: marc.carbonell@uib.es

³Departament de Física, Universitat de les Illes Balears, E-07122 Palma de Mallorca, Spain. Email: ramon.oliver@uib.es, joseluis.ballester@uib.es

ABSTRACT

Apart from the 11-year solar cycle, another periodicity around 155-160 days was discovered during solar cycle 21 in high energy solar flares, and its presence in sunspot areas and strong magnetic flux has been also reported. This periodicity has an elusive and enigmatic character, since it usually appears only near the maxima of solar cycles, and seems to be related with a periodic emergence of strong magnetic flux at the solar surface. Therefore, it is probably connected with the tachocline, a thin layer located near the base of the solar convection zone, where strong dynamo magnetic field is stored. We study the dynamics of Rossby waves in the tachocline in the presence of a toroidal magnetic field and latitudinal differential rotation. Our analysis shows that the magnetic Rossby waves are generally unstable and that the growth rates are sensitive to the magnetic field strength and to the latitudinal differential rotation parameters. Variation of the differential rotation and the magnetic field strength throughout the solar cycle enhance the growth rate of a particular harmonic in the upper part of the tachocline around the maximum of the solar cycle. This harmonic is symmetric with respect to the equator and has a period of 155-160 days. A rapid increase of the wave amplitude could give place to a magnetic flux emergence leading to observed periodicities in solar activity indicators related with magnetic flux.

Subject headings: Sun: oscillations —Physical Data and Processes: magnetic fields—MHD—waves

1. Introduction

During solar cycle 21, a short periodicity between 152–158 days was discovered in γ ray flares (Rieger et al. 1984), X ray flares (Rieger et al. 1984; Dennis 1985; Bai & Sturrock 1987; Kile & Cliver 1991; Dimitropoulou et al. 2008), flares producing energetic interplanetary electrons (Dröge et al. 1990), type II and IV radio bursts (Verma et al. 1991), and microwave flares (Bogart & Bai 1985; Kile & Cliver 1991). However, this periodicity was absent during solar cycle 22 (Kile & Cliver 1991; Bai 1992a; Özgüç & Ataç 1994).

The periodicity has also been detected in indicators of solar activity (sunspot blocking function, sunspot areas, “active” sunspot groups, group sunspot numbers) which suggest that it is associated preferentially with photospheric regions of compact magnetic field structures (Lean & Brueckner 1989; Lean 1990; Pap et al. 1990; Carbonell & Ballester 1990; Bouwer 1992; Carbonell & Ballester 1992; Verma et al. 1992; Oliver et al. 1998; Ballester et al. 1999; Krivova & Solanki 2002). Probably, the most important, and enigmatic, feature of the periodicity is that it appears during epochs of maximum activity and that it occurs in episodes of 1 to 3 years.

Rabin et al. (1991) performed a study of the magnetic flux variations during solar cycle 21 which reveals the existence of quasi-periodic pulses or episodes of enhanced magnetic activity. The duration of the pulses is ≈ 5 rotations during the years around maximum activity, the epoch in which the flare periodicity appears, and the comparison with magnetic field maps indicates that those pulses of activity correspond to the occurrence of complex active regions containing large sunspots (Bai 1987a).

Ballester et al. (2002, 2004) analyzed several data sets of, or strongly related to, photospheric magnetic flux to point out that the appearance of the near 160-day periodicity in different manifestations of solar activity during solar cycle 21 has its underlying cause in the appearance of the periodicity in the magnetic flux linked to regions of strong magnetic

field. They also showed that during solar cycle 22 the periodicity does not appear in the photospheric magnetic flux records and, as a consequence, the periodicity did not appear in other solar activity indicators, while during solar cycle 23 it appeared in the photospheric magnetic flux but not in other solar activity indicators.

Several mechanisms have been put forward in order to explain the existence of this periodicity. Wolff (1983) linked it to the interaction of rotating features (active longitude bands) resulting from g-modes with $l = 2$ and $l = 3$. Bai (1987b) suggested that the cause of this periodicity must be a mechanism that causes active regions to be more flare productive. Later, Bai & Sturrock (1987) concluded that it cannot be due to the interaction of “hot spots”, i.e. regions where flare activity is higher than elsewhere (Bai 1987a, 1988), rotating at different rates and that the cause must be a mechanism involving the whole Sun. Ichimoto et al. (1985) suggested that it is related to the timescale for storage and/or escape of magnetic fields in the solar convection zone. Bai & Cliver (1990), taking into account the possible intermittency of the periodicity, suggested that this behavior could be simulated with a damped, periodically forced non-linear oscillator, which shows periodic behavior for some values of the parameters and chaotic behavior for other values. Wolff (1992) argued that such periodicity can be understood in terms of the normal modes of oscillation of a nearly spherical, slowly rotating star, when two r-modes (inertial modes) couple with an interior g-mode beat. This suggestion seems to agree qualitatively with the fact that the periodicity is stronger around the activity maximum. Bai & Sturrock (1991) and Sturrock & Bai (1992) proposed that the Sun contains a “clock”, modeled by an oblique rotator or oscillator, with a period of 25.8 days and suggested that the periodicity of 154 days is just a subharmonic of that fundamental period. Later, Bai & Sturrock (1993) modified the earlier period to the value 25.50 days, but that model seems to be very constrained by helioseismological data about the rotation of the Sun’s interior. Lou (2000) suggested that such periodicities can be related to large-scale equatorially trapped

Rossby-type waves showing that, for typical solar parameters, the periods of these waves (with $n = 1$ and m even) are in good agreement with the observed ones. Moreover, Lou (2000) has also pointed out that such waves can give rise to detectable features, such as surface elevations in the photosphere. Coincidentally, Kuhn et al. (2000) have reported observations made with MDI onboard SOHO and claim to have detected a regular structure of 100-m “hills”, uniformly spaced over the surface of the Sun with a characteristic separation of 90,000 km. They suggest that this structure is the surface manifestation of Rossby waves, or r-modes oscillations. Finally, Dimitropoulou et al. (2008) have linked the found periodicities in different classes (B, C, M, X) of X-ray flares with the theoretical periods derived by Lou (2000), pointing out that odd m periodicities are also frequent and significant.

On the other hand, most of the proposed mechanisms to explain solar flares, specially the most energetic ones, accept as a prerequisite the emergence of magnetic flux (Priest 1990; Forbes 1991) which, by reconnection with the ambient field, triggers the destabilization of active regions. Based on this mechanism, Carbonell & Ballester (1990, 1992) suggested that the periodic increase in the occurrence rate of energetic flares is related to a periodic emergence of magnetic flux through the photosphere. Later, Oliver et al. (1998) showed that during solar cycle 21 there was a perfect time correlation between the intervals of occurrence of the periodicity in sunspot areas and energetic flares, and Ballester et al. (2002) clearly pointed out that in cycle 21, and during the time interval in which the periodicity appeared, there was a perfect time and frequency coincidence between the impulses of high-energy flares and those corresponding to strong photospheric magnetic flux. The efficiency of the reconnection mechanism depends on the geometry of the two flux systems (Galsgaard et al. 2007) and recent high resolution observations performed by Zuccarello et al. (2008) have confirmed the suitability of the mentioned mechanism for flare production.

Emerged magnetic flux is probably connected to deeper regions, namely to the tachocline, which is a thin, transition layer between differentially rotating convection zone and rigidly rotating radiative envelope. The tachocline may prevent the spreading of the solar angular momentum from the convection zone to the interior (Spiegel & Zahn 1992; Gough et al. 1998; Gough 2007; Garaud 2007) and probably it is the place, where the large-scale magnetic field which governs the solar activity is generated/amplified.

The observed periodicity of 155–160 days in the emerging flux is in the range of Rossby wave spectrum. Therefore, we suggest that the periodicity is connected to the Rossby wave activity in the tachocline. Rossby waves are well studied in the geophysical context (Gill 1982; Pedlosky 1987), however, the presence of magnetic fields significantly modifies their dynamics (Zaqarashvili et al. 2007, 2009). On the other hand, the differential rotation, which is inevitably present in the tachocline, may lead to the instability of particular harmonics of magnetic Rossby waves. It has been shown that the joint action of toroidal magnetic field and the differential rotation generally leads to tachocline instabilities (Gilman & Fox 1997; Cally 2003; Dikpati & Gilman 2005; Gilman & Cally 2007; Gilman et al. 2007). However, the stability analysis usually has been performed in an inertial frame, which complicates to extract the information about unstable Rossby modes. Therefore, it is of paramount importance to perform the stability analysis in a rotating frame. Another important point is that the consideration of a rotating frame may tighten the stability criteria as it has been suggested by Hughes & Tobias (2001). The difference between the present analysis and that by Hughes & Tobias (2001) is the inclusion of rotation which allows us to obtain Rossby wave solutions.

In this paper, we use a rotating spherical coordinate system to study the linear stability of magnetic Rossby waves in the solar tachocline taking into account the latitudinal differential rotation and the toroidal magnetic field. We perform a two dimensional

analysis, which can be followed in the future by more sophisticated shallow water considerations (Gilman 2000). We first derive the analytical conditions of instability similar to Dahlburg et al. (1998) and Hughes & Tobias (2001). Then, we perform a detailed stability analysis using Legendre polynomial expansions (Longuet-Higgins 1968) to obtain the spectrum of unstable harmonics of magnetic Rossby waves.

2. Magnetic Rossby wave equations in the presence of differential rotation and the toroidal magnetic field

Since the Rossby wave spectrum is clearly seen in the rotating frame, in the following we use a spherical coordinate system (r, θ, ϕ) rotating with the solar equator, where r is the radial coordinate, θ is the co-latitude and ϕ is the longitude.

The solar differential rotation law in general is

$$\Omega = \Omega_0 + \Omega_1(\theta), \tag{1}$$

with

$$\Omega_1(\theta) = -\Omega_0(s_2 \cos^2 \theta + s_4 \cos^4 \theta), \tag{2}$$

where Ω_0 is the equatorial angular velocity, and s_2, s_4 are constant parameters determined by observations.

Rossby waves are mainly polarized in the plane perpendicular to gravity, then a two-dimensional (θ, ϕ) analysis is a good approximation (Gill 1982). The two-dimensional analysis is also justified by Squire’s theorem which states that for each unstable 3-dimensional disturbance there is a corresponding unstable 2-dimensional disturbance with stronger growth rate (Squire 1933).

The magnetic field is predominantly toroidal, $\vec{B} = \Xi \hat{e}_\phi$, in the solar tachocline, and we take $\Xi = B_\phi(\theta) \sin \theta$, where B_ϕ is in general a function of co-latitude. Then, the

incompressible magnetohydrodynamic (MHD) equations in the frame rotating with Ω_0 are (see appendix A):

$$\frac{\partial u_\theta}{\partial t} + \Omega_1(\theta) \frac{\partial u_\theta}{\partial \phi} - 2[\Omega_0 + \Omega_1(\theta)] \cos \theta u_\phi = -\frac{1}{\rho R_0} \frac{\partial p_t}{\partial \theta} + \frac{B_\phi}{4\pi\rho R_0} \frac{\partial b_\theta}{\partial \phi} - 2\frac{B_\phi \cos \theta}{4\pi\rho R_0} b_\phi, \quad (3)$$

$$\begin{aligned} \frac{\partial u_\phi}{\partial t} + \Omega_1(\theta) \frac{\partial u_\phi}{\partial \phi} + 2\Omega_0 \cos \theta u_\theta + \Omega_1(\theta) \cos \theta u_\theta + u_\theta \frac{\partial}{\partial \theta} [\sin \theta \Omega_1(\theta)] = \\ = -\frac{1}{R_0 \sin \theta} \frac{\partial p_t}{\partial \phi} + \frac{B_\phi}{4\pi\rho R_0} \frac{\partial b_\phi}{\partial \phi} + \frac{b_\theta}{4\pi\rho R_0 \sin \theta} \frac{\partial}{\partial \theta} (B_\phi \sin^2 \theta), \end{aligned} \quad (4)$$

$$\frac{\partial b_\theta}{\partial t} + \Omega_1(\theta) \frac{\partial b_\theta}{\partial \phi} = \frac{B_\phi}{R_0} \frac{\partial u_\theta}{\partial \phi}, \quad \frac{\partial}{\partial \theta} (\sin \theta b_\theta) + \frac{\partial b_\phi}{\partial \phi} = 0, \quad (5)$$

$$\frac{\partial}{\partial \theta} (\sin \theta u_\theta) + \frac{\partial u_\phi}{\partial \phi} = 0, \quad (6)$$

where u_θ , u_ϕ , b_θ and b_ϕ are the velocity and magnetic field perturbations, p_t is the total pressure (hydrodynamic plus magnetic), ρ is the density and R_0 is the distance from the solar center to the tachocline.

We consider the stream functions for velocity and magnetic field

$$u_\theta = \frac{1}{\sin \theta} \frac{\partial \Psi}{\partial \phi}, \quad u_\phi = -\frac{\partial \Psi}{\partial \theta}, \quad b_\theta = \frac{1}{\sin \theta} \frac{\partial \Phi}{\partial \phi}, \quad b_\phi = -\frac{\partial \Phi}{\partial \theta}. \quad (7)$$

Substitution of expressions (7) into (3)-(6) and Fourier analysis with $\exp[im(\phi - ct)]$ gives

$$\begin{aligned} (c - \Omega_1) \left[\frac{\partial}{\partial \theta} \sin \theta \frac{\partial}{\partial \theta} - \frac{m^2}{\sin \theta} \right] \Psi - 2\Omega_0 \sin \theta \Psi + \frac{d}{d\theta} \left(\frac{1}{\sin \theta} \frac{d}{d\theta} (\Omega_1 \sin^2 \theta) \right) \Psi = \\ = -\frac{B_\phi}{4\pi\rho R_0} \left[\frac{\partial}{\partial \theta} \sin \theta \frac{\partial}{\partial \theta} - \frac{m^2}{\sin \theta} \right] \Phi + \frac{1}{4\pi\rho R_0} \frac{d}{d\theta} \left(\frac{1}{\sin \theta} \frac{d}{d\theta} (B_\phi \sin^2 \theta) \right) \Phi, \end{aligned} \quad (8)$$

$$(c - \Omega_1) \Phi = -\frac{B_\phi}{R_0} \Psi. \quad (9)$$

Let us now make the transformation of variables $\mu = \cos \theta$, then we obtain (Ψ and Φ are normalized by $\Omega_0 R_0$ and B_0 respectively, where B_0 is the value of B_ϕ at $\theta = 0$)

$$(\Omega_d - \omega) L \Psi + (2 - \frac{d^2}{d\mu^2} [\Omega_d (1 - \mu^2)]) \Psi - \beta^2 B L \Phi + \beta^2 \frac{d^2}{d\mu^2} [B (1 - \mu^2)] \Phi = 0 \quad (10)$$

$$(\Omega_d - \omega)\Phi = B\Psi, \quad (11)$$

where

$$L = \frac{\partial}{\partial\mu}(1 - \mu^2)\frac{\partial}{\partial\mu} - \frac{m^2}{1 - \mu^2}$$

is the Legendre operator and

$$\Omega_d(\mu) = \frac{\Omega_1(\mu)}{\Omega_0}, \quad \omega = \frac{c}{\Omega_0}, \quad \beta^2 = \frac{B_0^2}{4\pi\rho\Omega_0^2 R_0^2}, \quad B(\mu) = \frac{B_\phi(\mu)}{B_0}.$$

Eqs. (10)-(11) govern the 2-dimensional dynamics of magnetic Rossby waves in the presence of differential rotation and toroidal magnetic field. The equations are analogous to Eqs. (17)-(18) of Gilman & Fox (1997), but are written in the rotating frame instead of in the inertial one.

3. Analytical conditions of magnetic Rossby wave instability

In this section, we derive the analytical instability bounds using a well known technique (Howard 1961; Drazin & Reid 1981; Watson 1981; Gilman & Fox 1997; Dahlburg et al. 1998; Hughes & Tobias 2001).

Let us define a new function H

$$\Psi = (\Omega_d - \omega)H, \quad \Phi = BH.$$

Then Eqs. (10)-(11) can be cast in the following form

$$\frac{\partial}{\partial\mu}(1 - \mu^2)P(\mu)\frac{\partial H}{\partial\mu} - \frac{m^2}{1 - \mu^2}P(\mu)H + 2(\Omega_d - \omega)[1 + (\mu\Omega_d)']H - 2\beta^2 B(\mu B)'H = 0, \quad (12)$$

where

$$P(\mu) = (\Omega_d - \omega)^2 - \beta^2 B^2$$

and $'$ means differentiation with respect to μ .

Now, multiplying Eq. (12) by H^* , integrating from -1 to 1 and using the boundary conditions $H(\mu = \pm 1) = 0$, we get

$$\int_{-1}^1 P(\mu)Qd\mu - \int_{-1}^1 2(\Omega_d - \omega)[1 + (\mu\Omega_d)']|H|^2d\mu + \int_{-1}^1 2\beta^2B(\mu B)'|H|^2d\mu = 0, \quad (13)$$

where

$$Q = (1 - \mu^2) \left| \frac{\partial H}{\partial \mu} \right|^2 + \frac{m^2}{1 - \mu^2} |H|^2 > 0.$$

Considering $\omega = \omega_r + i\omega_i$ in Eq. (13) we obtain two different conditions for instability (see detailed derivations in appendix B). The first condition states that the instability takes place when

$$\omega_r^2 + \omega_i^2 \leq R_1^2, \quad (14)$$

with

$$R_1^2 = [(s_2\mu^2 + s_4\mu^4)^2 - \beta^2\mu^2]_{max}. \quad (15)$$

In the remaining $_{max}$ and $_{min}$ mean maximal and minimal values.

This means that the frequencies of unstable harmonics (actually phase speeds, while frequencies can be obtained by multiplying by m) lay inside the upper semicircle of complex ω -plane with center at the origin and radius R_1 (see Fig. 1).

The second instability condition is the semicircle theorem similar to Howard (1961). The MHD generalization of Howard's semicircle theorem in rectangular coordinates has been done by Dahlburg et al. (1998) and Hughes & Tobias (2001). Here the theorem is derived in the rotating spherical coordinate system as the second condition of instability (see details in appendix B), obtaining

$$\left(\omega_r - \frac{\Omega_{dmin} + \Omega_{dmax}}{2}\right)^2 + \omega_i^2 - \left(\frac{\Omega_{dmin} + \Omega_{dmax}}{2}\right)^2 + \Omega_{dmin}\Omega_{dmax} - A_{max} \leq 0, \quad (16)$$

where

$$A(\mu) = \frac{1 - \mu^2}{m^2}(\Omega_{dmin} + \Omega_{dmax} - 2\Omega_d)[1 + (\mu\Omega_d)'] + \frac{1 - \mu^2}{m^2}2\beta^2 B(\mu B)' - \beta^2 B^2. \quad (17)$$

We observe that $\Omega_{dmax} = 0$ and $\Omega_{dmin} = -\epsilon$, where $\epsilon = s_2 + s_4$, therefore we can write

$$\left(\omega_r + \frac{\epsilon}{2}\right)^2 + \omega_i^2 \leq \frac{\epsilon^2}{4} + A_{max}. \quad (18)$$

Due to this condition the frequencies of unstable modes lay inside the semicircle of the complex ω -plane with center

$$\left(-\frac{\epsilon}{2}, 0\right) \quad (19)$$

and radius (see Figure 1)

$$R_2 = \sqrt{\frac{\epsilon^2}{4} + A_{max}}. \quad (20)$$

Equations (14) and (18) are two necessary conditions of instability. They define two different semicircles in the complex ω -plane, and the instability occurs when the two semicircles overlap (see Hughes & Tobias (2001) for the same statement in the rectangular case). If the radius of one semicircle tends to zero, the instability disappears.

In the remaining we use a magnetic field

$$B_\phi = B_0\mu, \quad (21)$$

which changes sign at the equator (Gilman & Fox 1997).

Now, we may estimate the instability bounds under tachocline conditions. An important step is to choose the parameters of differential rotation, s_2 and s_4 . These

parameters are determined by observations and their values at the solar surface are $s_2 \approx s_4 \approx 0.14$. Helioseismology shows that the transition between the differentially rotating convective zone and the rigidly rotating radiative interior is described by the function $\Phi(r, r_c, w) = 0.5(1 + \text{erf}[2(r - r_c)/w])$, where erf is the error function, r_c is the radius of the central point of the tachocline and w is the characteristic thickness of the tachocline corresponding to a variation of $\Phi(r)$ from 0.08, at the bottom of the tachocline, to 0.92, at the tachocline's upper surface (Kosovichev 1996). In order to calculate the parameters of the differential rotation at the upper part of the tachocline, the solar surface values must be multiplied by 0.92, then, we obtain $s_2 \approx s_4 \approx 0.13$. However, it must be mentioned, that the real values of these parameters can be different in the tachocline (Charbonneau et al. 1999) and also can change through the solar cycle due to torsional oscillations (LaBonte & Howard 1982; Komm et al. 1993; Antia & Basu 2000; Howe et al. 2000; Howe 2009). Therefore, these values are tentative and further observations are needed to infer the correct parameters and their cycle dependence.

The typical values of equatorial angular velocity, radius and density in the tachocline are $\Omega_0 = 2.7 \cdot 10^{-6} \text{ s}^{-1}$, $R_0 = 5 \cdot 10^{10} \text{ cm}$ and $\rho = 0.2 \text{ g} \cdot \text{cm}^{-3}$ respectively. Then, the parameter β^2 is much smaller than unity being ≈ 0.0022 for a magnetic field strength of 10^4 G . Using these parameters we get $R_1 = 0.256$ and $R_2 = 0.154$ for azimuthal wave number $m = 1$. Then, the conditions (14) and (18) give that the minimum period of the $m = 1$ unstable modes in the tachocline is

$$T_{min} \approx 105 \text{ days.} \tag{22}$$

Therefore, only the magnetic Rossby modes with periods longer than 105 days may grow in time. However, equation (22) only gives a lower bound for oscillation periods. A more detailed analysis is required to reveal the spectrum of possible unstable harmonics.

4. Spectrum of unstable magnetic Rossby modes

In this section, we use the general technique of Legendre polynomial expansion (Longuet-Higgins 1968). Using the magnetic field profile (21), Eqs. (10)-(11) are rewritten as

$$(\Omega_d - \omega)L\Psi + \left(2 - \frac{d^2}{d\mu^2}[\Omega_d(1 - \mu^2)]\right)\Psi - \mu\beta^2 L\Phi - 6\mu\beta^2\Phi = 0 \quad (23)$$

$$(\Omega_d - \omega)\Phi = \mu\Psi. \quad (24)$$

Let us expand Ψ and Φ in infinite series of associated Legendre polynomials

$$\Psi = \sum_{n=m}^{\infty} a_n P_n^m(\mu), \quad \Phi = \sum_{n=m}^{\infty} b_n P_n^m(\mu), \quad (25)$$

which satisfy the boundary conditions $\Psi = \Phi = 0$ at $\mu = \pm 1$.

The latitude-dependent part of the differential rotation has the form

$$\Omega_d = -s_2\mu^2 - s_4\mu^4. \quad (26)$$

We substitute (25) into Eqs. (23)-(24) and, using a recurrence relation of Legendre polynomials, we obtain algebraic equations as infinite series (Details of the calculations can be found in Appendix C for the case when the differential rotation has only second order dependence on μ in expression (26)). The dispersion relation for the infinite number of harmonics can be obtained when the infinite determinant of the system is set to zero. In order to solve the determinant, we truncate the series at $n = 75$ and solve the resulting polynomial in ω numerically. The frequencies of different harmonics can be real or complex giving the stable or unstable character of a particular harmonic. It turns out that $m = 1$ harmonics are more unstable such as it has been systematically shown by previous works in many different occasions (Watson 1981; Gilman & Fox 1997; Dikpati & Gilman 2005; Gilman & Cally 2007).

Figure 2 shows the real, mc_r , and imaginary, mc_i , frequencies of all $m = 1$ unstable harmonics for different combinations of differential rotation parameters and magnetic field strength. In order to show the dependence on the parameters s_2, s_4 , we vary these parameters for different values of magnetic field strength so that the sum $s_2 + s_4$ (which is the difference in equatorial and polar angular velocities) remains 0.26. In Figure 2, the upper left panel corresponds to the case considered in Appendix C (i.e. $s_4 = 0$). Blue, green, yellow and red colors correspond to magnetic field strengths of $2 \cdot 10^3$ G, $6 \cdot 10^3$ G, $2 \cdot 10^4$ G and $4 \cdot 10^4$ G, respectively. Asterisks (circles) denote the symmetric (antisymmetric) harmonics with respect to the equator. The results show that the $s_4\mu^4$ term in the differential rotation (26) significantly affects the behaviour of unstable harmonics (Charbonneau et al. 1999). For each combination of s_2, s_4 and the magnetic field strength, there is a particular unstable harmonic with a growth rate much stronger than for the other harmonics. This harmonic is symmetric with respect to the equator and has the frequency of 0.17-0.18 Ω_0 (yielding periods of 150-160 days) for the magnetic field strength of $\leq 2 \cdot 10^4$ G. The frequency decreases for stronger magnetic fields (red colors), therefore Rieger-type periodicities arise as symmetric unstable harmonics for relatively weaker magnetic field strength.

Thus, the appearance of a strong oscillation with a particular frequency needs a suitable combination of differential rotation parameters (s_2, s_4) and magnetic field strength. However, the differential rotation parameters used in Figure 2 are probably too high for the solar tachocline. Therefore, we study the dependence of unstable harmonics on more realistic differential rotation rates.

Figure 3 displays the dependence of the most unstable symmetric harmonic (this harmonic can be identified on Fig. 2 as the blue, green, yellow and red asterisks at top of each panel) on the differential rotation parameters for two different values of the magnetic

field. Left panels correspond to the field strength of $2 \cdot 10^3$ G and right panels correspond to the strength of 10^4 G. Real and imaginary parts of the harmonic vs s_4 are plotted for different values of s_2 . The values of s_2 vary from 0.14 (blue color) to 0.09 (yellow color). We can observe that the frequency, mc_r , of this harmonic is only slightly dependent on the differential rotation parameters and takes values between 0.16-0.18 Ω_0 which correspond to oscillation periods of 150-170 days. This is the range where the Rieger-type periodicity has been observed. On the contrary, the growth rate, mc_i , of this harmonic strongly depends on the differential rotation parameters. The growth rate becomes stronger when both s_2 and s_4 , are increased.

The frequency and growth rate of this harmonic have no significant dependence on the magnetic field when its strength is smaller than 10^4 G. Figure 4 shows the dependence of the harmonic calculated for three different profiles of the differential rotation (blue line corresponds to $s_2 = 0.13$, $s_4 = 0.1$; the red line to $s_2 = 0.11$, $s_4 = 0.12$ and green line to $s_2 = 0.11$, $s_4 = 0.1$). We can observe that the stronger growth rate occurs for the red line, which means that s_4 is more important for the instability.

When the magnetic energy becomes comparable to the energy of differential rotation, then the frequency of the symmetric harmonic is significantly reduced (see red asterisks on Figure 2). The critical magnetic field strength, i.e. when the magnetic energy is comparable to the flow energy, is $\sim 5 \cdot 10^4$ G for the differential rotation parameters $s_2, s_4 = 0.13$. In this case, $(s_2 + s_4)^2 \sim \beta^2$, the radius of first semicircle R_1 (see Eq. (15)) tends to zero and the growth of symmetric unstable harmonics is suppressed.

5. Discussion

The periodicity of 155-160 days was discovered almost three decades ago, however the reason of its appearance/disappearance is still unknown. The most striking feature, perhaps, is its appearance only at certain times, which normally coincide with the maximum of the cycle (Figure 5). This coincidence naturally suggests that the magnetic field and the differential rotation at the solar cycle maximum provide suitable conditions for the appearance of this periodicity.

Here we show that the periodicity can be connected to the dynamics of magnetic Rossby waves in the tachocline, since, in this layer, they are unstable due to the presence of toroidal magnetic field and latitudinal differential rotation. First, we have derived the analytical bounds of instability, which state that $m = 1$ unstable modes have periods > 105 days. Next, we have calculated the detailed spectrum of unstable harmonics using the method of Legendre polynomial expansion. We have found that the behaviour of unstable harmonics is very sensitive to the combination of magnetic field strength and the differential rotation parameters (s_2, s_4). Each combination of the parameters favours a particular harmonic, which has stronger growth rate compared to other unstable harmonics. Therefore, this harmonic may quickly dominate over the others and may lead to a detectable oscillation, if the parameters remain more or less unchanged during some time. Unstable harmonics have two types of symmetry with respect to the equator: symmetric and antisymmetric. The growth rates of symmetric modes are higher than the antisymmetric ones and they depend on the differential rotation parameters; the growth becomes stronger for stronger shear.

Frequencies of symmetric unstable modes are in the range $0.16-0.18 \Omega_0$ (Figure 3), which yield the periods of 150-170 days. In the case of strong differential rotation, their growth rate may reach up to $0.015 \Omega_0$ i.e. the growth time is ~ 280 days. Therefore, they may quickly dominate over the rest. The growth of the magnetic Rossby wave amplitude

leads to an enhanced magnetic buoyancy at the tachocline which causes the periodic eruption of magnetic flux towards the solar surface. Therefore, the periodicity is observed in the emerged magnetic flux and consequently in many indicators of solar activity (see references in the Introduction).

The question why the periodicities appear only at particular times (mostly just after solar maximum, see Figure 5) needs additional explanation. A possible reason is that the growth of symmetric harmonics strongly depends on the differential rotation parameters (s_2, s_4). It is known that the solar differential rotation is changing through the solar cycle. The pattern known as the torsional oscillation has been first observed at the solar surface in full disc velocity measurements (LaBonte & Howard 1982) and later in surface magnetic features as well (Komm et al. 1993). Helioseismology shows that the torsional oscillation is not only a surface phenomenon but may penetrate deeper into the solar interior (Antia & Basu 2000; Howe et al. 2000; Howe 2009). Then, the parameters s_2, s_4 may vary through the solar cycle in the tachocline, which permits the strong growth of symmetric magnetic Rossby waves only at particular times. This time should coincide with the solar maximum. We think that additional helioseismic estimations are needed to study this phenomenon.

One of the significant simplifications in our approach is the linear stability analysis. The growth of perturbation amplitudes probably leads to nonlinear effects. On the other hand, the process would be accompanied by increased magnetic buoyancy, which causes the eruption of magnetic flux upwards and consequently may stop further growth of amplitudes. These processes should be studied with sophisticated numerical simulations in the future.

It should be mentioned here that numerous previous papers have studied the tachocline instabilities (Gilman & Fox 1997; Cally 2003; Dikpati & Gilman 2005; Gilman & Cally 2007; Gilman et al. 2007). However, all the calculations have been performed in an inertial

frame, while the Rossby wave dynamics is more clearly seen in a rotating frame. Another important difference between inertial and rotating frames is that the instability conditions may be tightened in the moving frame as suggested by Hughes & Tobias (2001).

The solar tachocline may consist of two parts: the inner radiative layer with a strongly stable stratification and the outer overshoot layer with a weakly stable stratification (Gilman 2000). The latitudinal differential rotation should be stronger in the upper tachocline and weaker in the lower one. On the contrary, the magnetic field strength should be higher in the lower part and smaller in the upper one. Therefore, the upper tachocline may favor the better conditions for the growth of symmetric unstable harmonics, which trigger the Rieger-type periodicities.

6. Conclusions

In summary, we have shown that the destabilization of magnetic Rossby waves in the solar tachocline is produced by the joint effect of the latitudinal differential rotation and the toroidal magnetic field. The frequencies and growth rates of unstable harmonics depend on the combination of the differential rotation parameters and the magnetic field strength. The possible increase of latitudinal differential rotation at the solar maximum may trigger the instability of symmetric harmonic with period of 155-160 days in the upper part of the tachocline. This instability has a direct correlation with magnetic flux emergence, therefore the periodicity also appears in solar activity indicators related with magnetic flux. Later on, and probably via reconnection, this periodic magnetic flux emergence triggers the observed periodicity in solar flares.

The magnetic Rossby wave theory opens a new research area about the activity on the Sun and other stars, and magnetic Rossby waves can be of paramount importance for

observed intermediate periodicities in solar and stellar activity (Massi et al. 1998, 2005).

Acknowledgements The authors acknowledge the financial support provided by MICINN and FEDER funds under grant AYA2006-07637. Also, the Conselleria d’Economia, Hisenda i Innovació of the Government of the Balearic Islands is gratefully acknowledged for the funding provided under grant PCTIB2005GC3-03. T. V. Z. acknowledges financial support from the Austrian Fond zur Förderung der wissenschaftlichen Forschung (under project P21197-N16), the Georgian National Science Foundation (under grant GNSF/ST06/4-098) and the Universitat de les Illes Balears. Wavelet software was provided by C. Torrence and G. Compo ¹.

A. MHD equations in a rotating frame

In the case of rigid rotation it is straightforward to transform equations from inertial into the rotational frame, but the presence of differential rotation slightly complicates the considerations as different parts of the Sun rotate with different angular velocity. The best way to overcome the difficulty is to consider the frame rotating with the equator. Then the latitudinal differential rotation can be considered as the unperturbed shearing motion in this frame. 2-dimensional incompressible linearised MHD Equations (θ, ϕ -plane) in the frame rotating with angular velocity of the equator, Ω_0 , are

$$\frac{\partial u_\theta}{\partial t} + \frac{U_\phi}{R_0 \sin \theta} \frac{\partial u_\theta}{\partial \phi} - 2\Omega_0 \cos \theta u_\phi - 2 \frac{\cos \theta}{R_0 \sin \theta} U_\phi u_\phi = -\frac{1}{\rho R_0} \frac{\partial p_t}{\partial \theta} + \frac{\Xi}{4\pi \rho R_0 \sin \theta} \frac{\partial b_\theta}{\partial \phi} - 2 \frac{\Xi}{4\pi \rho R_0} \frac{\cos \theta}{\sin \theta} b_\phi, \quad (\text{A1})$$

$$\begin{aligned} \frac{\partial u_\phi}{\partial t} + \frac{U_\phi}{R_0 \sin \theta} \frac{\partial u_\phi}{\partial \phi} + \frac{u_\theta}{R_0} \frac{\partial U_\phi}{\partial \theta} + 2\Omega_0 \cos \theta u_\theta + \frac{\cos \theta}{R_0 \sin \theta} u_\theta U_\phi = \\ = -\frac{1}{R_0 \sin \theta} \frac{\partial p_t}{\partial \phi} + \frac{\Xi}{4\pi \rho R_0 \sin \theta} \frac{\partial b_\phi}{\partial \phi} + \frac{b_\theta}{4\pi \rho R_0 \sin \theta} \frac{\partial}{\partial \theta} (\Xi \sin \theta), \end{aligned} \quad (\text{A2})$$

¹The software is available at <http://paos.colorado.edu/research/wavelets>

$$\frac{\partial b_\theta}{\partial t} + \frac{U_\phi}{R_0 \sin \theta} \frac{\partial b_\theta}{\partial \phi} = \frac{\Xi}{R_0 \sin \theta} \frac{\partial u_\theta}{\partial \phi}, \quad (\text{A3})$$

$$\frac{\partial}{\partial \theta} (\sin \theta u_\theta) + \frac{\partial U_\phi}{\partial \phi} = 0, \quad (\text{A4})$$

$$\frac{\partial}{\partial \theta} (\sin \theta b_\theta) + \frac{\partial b_\phi}{\partial \phi} = 0, \quad (\text{A5})$$

where u_θ , u_ϕ , b_θ and b_ϕ are the velocity and magnetic field perturbations, Ξ and U_ϕ are azimuthal components of unperturbed magnetic field and velocity in the rotating frame, p_t is the perturbation in total (hydrodynamic plus magnetic) pressure.

We consider U_ϕ as the differential rotation with respect to the equator, i.e.

$$U_\phi = R_0 \sin \theta \Omega_1(\theta). \quad (\text{A6})$$

Substitution of this expression into Eqs. (A1)-(A5) gives Eqs. (3)-(6).

B. Derivation of analytical instability conditions

The real and imaginary parts of Eq. (13) with $\omega = \omega_r + i\omega_i$ are

$$\int_{-1}^1 [(\Omega_d - \omega_r)^2 - \omega_i^2 - \beta^2 B^2] Q d\mu - \int_{-1}^1 2(\Omega_d - \omega_r)[1 + (\mu\Omega_d)'] |H|^2 d\mu + \int_{-1}^1 2\beta^2 B(\mu B)' |H|^2 d\mu = 0 \quad (\text{B1})$$

and

$$2i\omega_i \left[\int_{-1}^1 (\Omega_d - \omega_r) Q d\mu - \int_{-1}^1 [1 + (\mu\Omega_d)'] |H|^2 d\mu \right] = 0. \quad (\text{B2})$$

Unstable harmonics should have non zero ω_i , therefore Eq. (B2) requires

$$\int_{-1}^1 (\Omega_d - \omega_r) Q d\mu = \int_{-1}^1 [1 + (\mu\Omega_d)'] |H|^2 d\mu.$$

Substitution of $\int_{-1}^1 \Omega_d Q d\mu$ from this equation into Eq. (B1) leads to the equation

$$\int_{-1}^1 [\Omega_d^2 - \omega_r^2 - \omega_i^2 - \beta^2 B^2] Q d\mu - \int_{-1}^1 2\Omega_d [1 + (\mu\Omega_d)'] |H|^2 d\mu + \int_{-1}^1 2\beta^2 B(\mu B)' |H|^2 d\mu = 0, \quad (\text{B3})$$

which then can be rewritten as

$$\int_{-1}^1 [\Omega_d^2 - \omega_r^2 - \omega_i^2 - \beta^2 B^2] (1 - \mu^2) \left| \frac{\partial H}{\partial \mu} \right|^2 d\mu + \int_{-1}^1 \left[\Omega_d^2 - \omega_r^2 - \omega_i^2 - \beta^2 B^2 - 2\Omega_d [1 + (\mu\Omega_d)'] \frac{1 - \mu^2}{m^2} + 2\beta^2 B(\mu B)' \frac{1 - \mu^2}{m^2} \right] \frac{m^2}{1 - \mu^2} |H|^2 d\mu = 0.$$

This equation will be satisfied if both integrals are zero, which requires

$$(\Omega_d^2 - \beta^2 B^2)_{min} \leq \omega_r^2 + \omega_i^2 \leq (\Omega_d^2 - \beta^2 B^2)_{max} \quad (\text{B4})$$

and

$$\left(\Omega_d^2 - \beta^2 B^2 - 2\Omega_d [1 + (\mu\Omega_d)'] \frac{1 - \mu^2}{m^2} + 2\beta^2 B(\mu B)' \frac{1 - \mu^2}{m^2} \right)_{min} \leq \omega_r^2 + \omega_i^2 \leq \left(\Omega_d^2 - \beta^2 B^2 - 2\Omega_d [1 + (\mu\Omega_d)'] \frac{1 - \mu^2}{m^2} + 2\beta^2 B(\mu B)' \frac{1 - \mu^2}{m^2} \right)_{max}. \quad (\text{B5})$$

The inequality (B5) is similar to the inequality (B4), but with two additional terms in the left and right hand sides. Both additional terms are positive, therefore, inequality (B4) determines a condition of instability. Using the profiles of magnetic field (21) and the differential rotation (2), Eq. (B4) leads to Eq. (14) in the main text.

In order to obtain the semicircle theorem let us observe that

$$\int_{-1}^1 (\Omega_d - \Omega_{dmin})(\Omega_d - \Omega_{dmax}) Q d\mu \leq 0. \quad (\text{B6})$$

Then the substitution of $\int_{-1}^1 \Omega_d^2 Q d\mu$ from Eq. (B3) into Eq. (B6) gives

$$\int_{-1}^1 [\omega_r^2 + \omega_i^2 + \beta^2 B^2 - (\Omega_{dmin} + \Omega_{dmax})\omega_r + \Omega_{dmin}\Omega_{dmax}] Q d\mu \leq$$

$$\int_{-1}^1 (\Omega_{dmin} + \Omega_{dmax} - 2\Omega_d)[1 + (\mu\Omega_d)']|H|^2 d\mu + \int_{-1}^1 2\beta^2 B(\mu B)'|H|^2 d\mu.$$

This inequality can be rewritten as

$$\begin{aligned} & \int_{-1}^1 \left[\left(\omega_r - \frac{\Omega_{dmin} + \Omega_{dmax}}{2} \right)^2 + \omega_i^2 + \beta^2 B^2 - \left(\frac{\Omega_{dmin} + \Omega_{dmax}}{2} \right)^2 + \Omega_{dmin} \Omega_{dmax} \right] (1 - \mu^2) \left| \frac{\partial H}{\partial \mu} \right|^2 d\mu + \\ & + \int_{-1}^1 \left[\left(\omega_r - \frac{\Omega_{dmin} + \Omega_{dmax}}{2} \right)^2 + \omega_i^2 + \beta^2 B^2 - \left(\frac{\Omega_{dmin} + \Omega_{dmax}}{2} \right)^2 + \Omega_{dmin} \Omega_{dmax} - \right. \\ & \left. - \frac{1 - \mu^2}{m^2} (\Omega_{dmin} + \Omega_{dmax} - 2\Omega_d)[1 + (\mu\Omega_d)'] - \frac{1 - \mu^2}{m^2} 2\beta^2 B(\mu B)' \right] \frac{m^2}{1 - \mu^2} |H|^2 d\mu \leq 0. \quad (\text{B7}) \end{aligned}$$

At least, one of the two integrals should have negative sign, therefore

$$\left(\omega_r - \frac{\Omega_{dmin} + \Omega_{dmax}}{2} \right)^2 + \omega_i^2 + (\beta^2 B^2)_{min} - \left(\frac{\Omega_{dmin} + \Omega_{dmax}}{2} \right)^2 + \Omega_{dmin} \Omega_{dmax} \leq 0 \quad (\text{B8})$$

and/or

$$\left(\omega_r - \frac{\Omega_{dmin} + \Omega_{dmax}}{2} \right)^2 + \omega_i^2 - \left(\frac{\Omega_{dmin} + \Omega_{dmax}}{2} \right)^2 + \Omega_{dmin} \Omega_{dmax} - A_{max} \leq 0, \quad (\text{B9})$$

where

$$A(\mu) = \frac{1 - \mu^2}{m^2} (\Omega_{dmin} + \Omega_{dmax} - 2\Omega_d)[1 + (\mu\Omega_d)'] + \frac{1 - \mu^2}{m^2} 2\beta^2 B(\mu B)' - \beta^2 B^2. \quad (\text{B10})$$

The inequality (B9) is wider than (B8). Therefore, it determines the second condition of instability (Eq. (16) in the main text).

C. Derivation of dispersion equations using Legendre polynomial expansion

The substitution of (25) into Eqs. (23)-(24) and using the Legendre equation

$$LP_n^m + n(n+1)P_n^m = 0 \text{ leads to}$$

$$-(\Omega_d - \omega) \sum_{n=m}^{\infty} n(n+1)a_n P_n^m + \left(2 - \frac{d^2}{d\mu^2} [\Omega_d(1 - \mu^2)]\right) \sum_{n=m}^{\infty} a_n P_n^m + \mu\beta^2 \sum_{n=m}^{\infty} n(n+1)b_n P_n^m -$$

$$-6\mu\beta^2 \sum_{n=m}^{\infty} b_n P_n^m = 0, \quad (\text{C1})$$

$$(\Omega_d - \omega) \sum_{n=m}^{\infty} b_n P_n^m = \mu \sum_{n=m}^{\infty} a_n P_n^m. \quad (\text{C2})$$

Now we take the explicit form of $\Omega_d = -\epsilon\mu^2$, then

$$\sum_{n=m}^{\infty} [\omega n(n+1) + 2 + 2\epsilon] a_n P_n^m + \epsilon \sum_{n=m}^{\infty} [n(n+1) - 12] a_n \mu^2 P_n^m + \beta^2 \sum_{n=m}^{\infty} [n(n+1) - 6] b_n \mu P_n^m = 0, \quad (\text{C3})$$

$$\sum_{n=m}^{\infty} a_n \mu P_n^m + \sum_{n=m}^{\infty} \omega b_n P_n^m + \epsilon \sum_{n=m}^{\infty} b_n \mu^2 P_n^m = 0. \quad (\text{C4})$$

We use the recurrence relations between Legendre polynomials, namely:

$$\mu^2 P_n^m = A_n P_{n-2}^m + B_n P_n^m + C_n P_{n+2}^m,$$

$$\mu P_n^m = D_n P_{n-1}^m + E_n P_{n+1}^m,$$

where

$$A_n = \frac{(n+m)(n+m-1)}{(2n+1)(2n-1)}, \quad B_n = \frac{(n-m)(n+m)}{(2n+1)(2n-1)} + \frac{(n-m+1)(n+m+1)}{(2n+1)(2n+3)},$$

$$C_n = \frac{(n-m+1)(n-m+2)}{(2n+1)(2n+3)}, \quad D_n = \frac{n+m}{2n+1}, \quad E_n = \frac{n-m+1}{2n+1}.$$

Substitution of these relations into Eqs. (C3)-(C4) gives

$$\begin{aligned} & \sum_{n=m}^{\infty} [\omega n(n+1) + 2 + 2\epsilon] a_n P_n^m + \epsilon \sum_{n=m}^{\infty} [n(n+1) - 12] A_n a_n P_{n-2}^m + \epsilon \sum_{n=m}^{\infty} [n(n+1) - 12] B_n a_n P_n^m + \\ & + \epsilon \sum_{n=m}^{\infty} [n(n+1) - 12] C_n a_n P_{n+2}^m + \beta^2 \sum_{n=m}^{\infty} [n(n+1) - 6] D_n b_n P_{n-1}^m + \beta^2 \sum_{n=m}^{\infty} [n(n+1) - 6] E_n b_n P_{n+1}^m = 0, \\ & \sum_{n=m}^{\infty} a_n D_n P_{n-1}^m + \sum_{n=m}^{\infty} a_n E_n P_{n+1}^m + \sum_{n=m}^{\infty} \omega b_n P_n^m + \epsilon \sum_{n=m}^{\infty} A_n b_n P_{n-2}^m + \epsilon \sum_{n=m}^{\infty} B_n b_n P_n^m + \epsilon \sum_{n=m}^{\infty} C_n b_n P_{n+2}^m = 0. \end{aligned}$$

Rearranging terms we obtain

$$\begin{aligned}
& \sum_{n=m}^{\infty} [\omega n(n+1)+2+2\epsilon] a_n P_n^m + \epsilon \sum_{n=m}^{\infty} [(n+2)(n+3)-12] A_{n+2} a_{n+2} P_n^m + \epsilon \sum_{n=m}^{\infty} [n(n+1)-12] B_n a_n P_n^m + \\
& + \epsilon \sum_{n=m}^{\infty} [(n-2)(n-1)-12] C_{n-2} a_{n-2} P_n^m + \beta^2 \sum_{n=m}^{\infty} [(n+1)(n+2)-6] b_{n+1} D_{n+1} P_n^m + \\
& + \beta^2 \sum_{n=m}^{\infty} [n(n-1)-6] b_{n-1} E_{n-1} P_n^m = 0, \\
& \sum_{n=m}^{\infty} a_{n+1} D_{n+1} P_n^m + \sum_{n=m}^{\infty} a_{n-1} E_{n-1} P_n^m + \sum_{n=m}^{\infty} \omega b_n P_n^m + \epsilon \sum_{n=m}^{\infty} A_{n+2} b_{n+2} P_n^m + \epsilon \sum_{n=m}^{\infty} B_n b_n P_n^m + \\
& + \epsilon \sum_{n=m}^{\infty} C_{n-2} b_{n-2} P_n^m = 0.
\end{aligned}$$

Now the coefficients of P_n^m give the equations

$$S_n a_n + F_n a_{n+2} + G_n a_{n-2} + H_n b_{n+1} + I_n b_{n-1} = 0, \quad (\text{C5})$$

$$J_n a_{n+1} + K_n a_{n-1} + Q_n b_n + P_n b_{n+2} + M_n b_{n-2} = 0, \quad (\text{C6})$$

where

$$\begin{aligned}
S_n &= \omega n(n+1)+2+2\epsilon + \epsilon [n(n+1)-12] \frac{(n-m)(n+m)}{(2n+1)(2n-1)} + \epsilon [n(n+1)-12] \frac{(n-m+1)(n+m+1)}{(2n+1)(2n+3)}, \\
F_n &= \epsilon [(n+2)(n+3)-12] \frac{(n+m+2)(n+m+1)}{(2n+5)(2n+3)}, \quad G_n = \epsilon [(n-2)(n-1)-12] \frac{(n-m-1)(n-m)}{(2n-3)(2n-1)}, \\
H_n &= \beta^2 [(n+1)(n+2)-6] \frac{n+m+1}{2n+3}, \quad I_n = \beta^2 [n(n-1)-6] \frac{n-m}{2n-1}, \quad J_n = \frac{n+m+1}{2n+3}, \\
K_n &= \frac{n-m}{2n-1}, \quad Q_n = \omega + \epsilon \frac{(n-m)(n+m)}{(2n+1)(2n-1)} + \epsilon \frac{(n-m+1)(n+m+1)}{(2n+1)(2n+3)}, \\
P_n &= \epsilon \frac{(n+m+2)(n+m+1)}{(2n+5)(2n+3)}, \quad M_n = \epsilon \frac{(n-m-1)(n-m)}{(2n-3)(2n-1)}.
\end{aligned}$$

The expressions (C5)-(C6) are infinite series and the dispersion relation for the infinite number of harmonics can be obtained when the infinite determinant of the system is zero. In order to solve the determinant, we cut the series at $n = 75$ and solve the resulting polynomial in ω numerically.

REFERENCES

- Antia, H. M. & Basu, S. 2000, *ApJ*, 541, 442
- Bai, T. 1987a, *ApJ*, 314, 795
- Bai, T. 1987b, *ApJ*, 318, L85
- Bai, T. 1988, *ApJ*, 328, 860
- Bai, T. 1992a, *ApJ*, 388, L69
- Bai, T. 1992b, *ApJ*, 397, 584
- Bai, T., & Cliver, E. H. 1990, *ApJ*, 363, 299
- Bai T., & Sturrock P. 1987, *Nature*, 327, 601
- Bai T., & Sturrock P. 1991, *Nature*, 350, 141
- Bai T., & Sturrock P. 1993, *ApJ*, 409, 486
- Ballester, J. L., Oliver, R., & Baudin, F. 1999, *ApJ*, 522, L153
- Ballester, J. L., Oliver, R. & Carbonell, M. 2002, *ApJ*, 566, 505
- Ballester, J. L., Oliver, R. & Carbonell, M. 2004, *ApJ*, 615, L173
- Bogart, R. S., & Bai T. 1985, *ApJ*, 299, L51
- Bouwer, S. D. 1992, *Sol. Phys.*, 142, 365
- Cally, P. S. 2003, *MNRAS*, 339, 957
- Canfield, R. C., Blais, K. A., McClymont, A. N., Metcalf, T. R., Reardon, K. P., Wülser, J. P., Acton, L. W., Kurokawa, H., & Hirayama, T. 1993, *X-Ray Solar Physics from*

- Yohkoh, Uchida, Y., Watanabe, T., Shibata, K., & Hudson, H. S., Tokyo: Universal Academy Press, 153
- Carbonell, M., & Ballester, J. L. 1990, *A&A*, 238, 377
- Carbonell, M., & Ballester, J. L. 1992, *A&A*, 255, 350
- Charbonneau, P., Dikpati, M. & Gilman, P.A. 1999, *ApJ*, 526, 523
- Dahlburg, R. B., Boncinelli, P. & Einaudi, G. 1998, *Phys. Plasmas*, 5, 79
- Dennis, B. R. 1985, *Sol. Phys.*, 100, 465
- Dikpati, M. & Gilman, P. A. 2005, *ApJ*, 635, L193
- Drazin, P.G. & Reid, W.H., 1981, *Hydrodynamic stability*, (Cambridge: Cambridge University Press)
- Dröge, W., Gibbs, K., Grunsfeld, J. M., Meyer, P., Newport, B. J., Evenson, P., & Moses, D. 1990, *ApJS*, 73, 279
- Dimitropoulou, M., Moussas, X., & Strintzi, D. 2008, *MNRAS*, 386, 2278
- Forbes, T. G. 1991, *Geophys. Astrophys. Fluid Dynamics*, 62, 15
- Galsgaard, K., Archontis, V., Moreno-Insertis, F., & Hood, A. W. 2007, *ApJ*, 666, 516
- Garaud, P. 2007, in *The Solar Tachocline*, ed. D.W. Hughes, R. Rosner & N.O. Weiss (Cambridge: Cambridge University Press), 147
- Gill, A. E. 1982, *Atmosphere-Ocean Dynamics*, San Diego: Academic Press
- Gilman, P. A. & Fox, P. A. 1997, *ApJ*, 484, 439
- Gilman, P.A. 2000, *ApJ*, 484, 439

- Gilman, P.A., & Cally, P.S. 2007, in *The Solar Tachocline*, ed. D.W. Hughes, R. Rosner & N.O. Weiss (Cambridge: Cambridge University Press), 243
- Gilman, P.A., Dikpati, M. & Miesch, M.S., 2007, *ApJS*, 170, 203
- Gough, D.O. & McIntyre, M.E. 1998, *Nature*, 394, 755
- Gough, D. 2007, in *The Solar Tachocline*, ed. D.W. Hughes, R. Rosner & N.O. Weiss (Cambridge: Cambridge University Press), 3
- Howard, L. N. 1961, *J. Fluid. Mech.*, 13, 158
- Howe, R., Christensen-Dalsgaard, J., Hill, F., Komm, R.W., Larsen, R.M., Schou, J., Thompson, M.J. & Toomre, J. 2000, *ApJ*, 533, L163
- Howe, R. 2009, *Living Reviews in Solar Physics*, 6, 1
(<http://www.livingreviews.org/lrsp-2009-1>)
- Hoyt, D. V., & Schatten, K. H. 1998, *Sol. Phys.*, 181, 491
- Hughes, D.W. & Tobias, S.M. 2001, *Proc. R. Soc. Lond. A*, 457, 1365
- Ichimoto, K., Kubota, J., Suzuki, M., Tohmura, I., & Kurokawa, H. 1985, *Nature*, 316, 422
- Kile, J. N., & Cliver, E. W. 1990, *ApJ*, 370, 442
- Komm, R. W., Howard, R. F. & Harvey, J. W. 1993, *Solar Phys.*, 143, 19
- Kosovichev, A. G. 1996, *ApJ*, 469, L61
- Krivova, N. A., & Solanki, S. 2002, *A&A*, 701
- Kuhn, J., Armstrong, J. D., Bush, R. I., & Scherrer, P. 2000, *Nature*, 405, 544
- LaBonte, B.J. & Howard, R. 1982, *Solar Phys.*, 75, 16

- Lean, J. L. 1990, ApJ, 363, 718
- Lean, J., & Brueckner, G. E. 1989, ApJ, 337, 568
- Longuet-Higgins, M.S., 1965, Proceedings of The Royal Society Series / A, 284, 40
- Longuet-Higgins, M. S. 1968, Proc. R. Soc. London. A, 262, 511
- Lou, Y. Q. 2000, ApJ, 540, 1102
- Massi, M., Neidhöfer, J., Torricelli-Ciamponi, G. & Chiuderi-Drago, F. 1998, A&A, 332, 149
- Massi, M., Neidhöfer, J., Carpentier, Y. & Ros, E. 2005, A&A, 435, L1
- Oliver, R., Ballester, J. L., & Baudin, F. 1998, Nature, 394, 552
- Özgüç, A. & Ataç, T. 1994, Sol. Phys., 150, 339
- Pap, J., Tobiska, W. K., & Bouwer, S. D. 1990, Sol. Phys.129, 165
- Pedlosky, J. 1987, Geophysical Fluid Dynamics (New York: Springer)
- Priest, E. R. 1990, Basic Plasma Processes on the Sun, Priest, E. R., & Krishnan, V., Dordrecht: Kluwer Academic Publishers, 271
- Rabin, D. M., DeVore, C. R., Sheeley, N. R., Harvey, K. L., & Hoeksema, J. T. 1991, Solar Interior and Atmosphere, Cox, A. C., Livingston, W. C., & Matthews, M. S., Tucson: The Universe of Arizona Press, 781
- Rieger, E., Share, G. H., Forrest, D. J., Kanbach, G., Reppin, C., & Chupp, E. L. 1984, Nature, 312, 623
- Spiegel, E.A. & Zahn, J.-P. 1992, A&A, 265

- Squire, H.B. 1933, Proc. R. Soc. Lond. A, 142, 621
- Sturrock, P., & Bai, T. 1992, ApJ, 397, 337
- Torrence, C., & Compo, G. P. 1998, Bull. Amer. Meteor. Soc., 79, 61
- Verma, V. K., Joshi, G. C., Wahab Uddin, & Paliwal, D. C. 1991, A&AS, 90, 83
- Verma, V. K., Joshi, G. C., & Paliwal, D. C. 1992, Sol. Phys., 138, 205
- Watson, M. 1981, Geophys. Astrophys. Fluid dynamics, 16, 285
- Wolff, C. L. 1983, ApJ, 264, 667
- Wolff, C. L. 1992, Sol. Phys., 142, 187
- Zaqarashvili, T. V., Oliver, R., Ballester, J. L. & Shergelashvili, B. M. 2007, A&A, 470, 815
- Zaqarashvili, T. V., Oliver, R. & Ballester, J. L. 2009, ApJ, 691, L41
- Zuccarello, F., Battiato, V., Contarino, L., Guglielmino, S., Romano, P. & Spadaro, D.
2008, A&A, 488, 1117

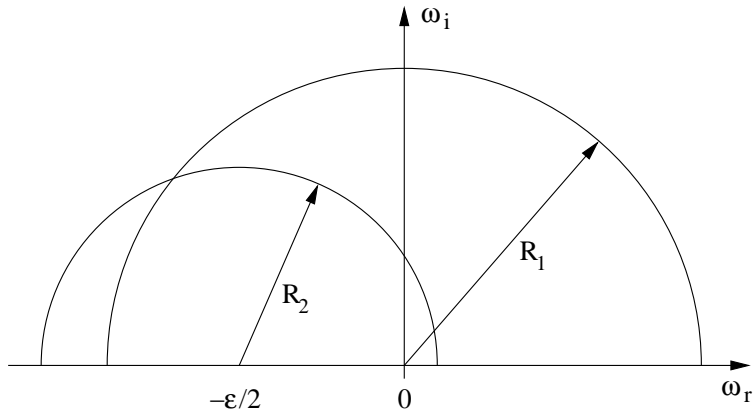


Fig. 1.— Semicircles of unstable harmonics in the complex (ω_r, ω_i) -plane corresponding to the two instability conditions, Eqs. (14) and (18). Instability occurs when these two semicircles overlap. ω_r, ω_i, R_1 and R_2 are normalised with respect to Ω_0 .

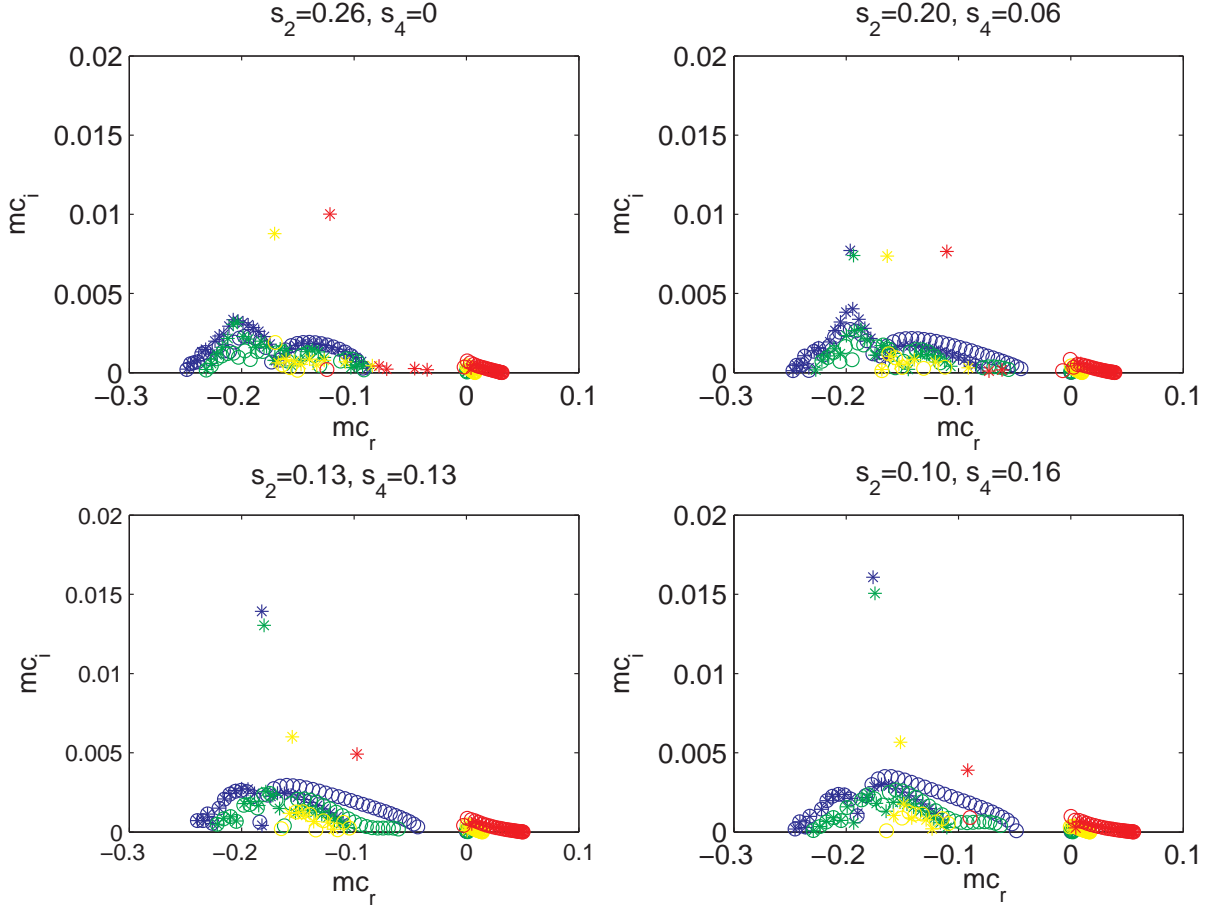


Fig. 2.— Real (mc_r) vs imaginary (mc_i) parts of unstable harmonic frequencies for different combinations of differential rotation parameters s_2 , s_4 and magnetic field strengths (frequency is normalized by equatorial angular velocity, Ω_0). Note that the difference between equatorial and polar angular velocities $s_2 + s_4 = 0.26$ remains the same for all panels. The toroidal wave number m equals 1. Blue, green, yellow and red colors correspond to magnetic field strengths of $2 \cdot 10^3$ G, $6 \cdot 10^3$ G, $2 \cdot 10^4$ G and $4 \cdot 10^4$ G, respectively. Asterisks denote the symmetric harmonics with respect to the equator, while circles denote the antisymmetric ones. The frequencies are normalized by equatorial angular velocity, Ω_0 ; for example, $mc_r = 0.18$ corresponds to the period of ~ 150 days.

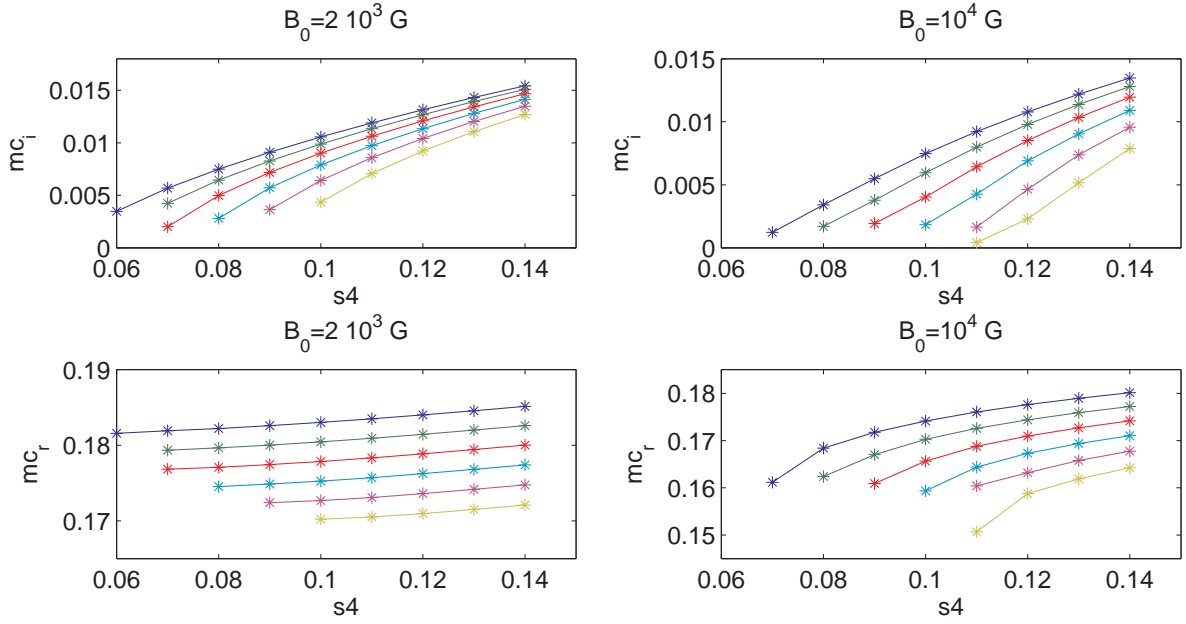


Fig. 3.— Real (lower panels) and imaginary (upper panels) part of the frequency of the most unstable symmetric harmonic vs s_4 for different values of s_2 . Dark blue, green, red, blue, magenta and yellow colors correspond to 0.14, 0.13, 0.12, 0.11, 0.10 and 0.09 s_2 values respectively. The magnetic field strength equals to $2 \cdot 10^3$ G (left panels) and 10^4 G (right panel) respectively.

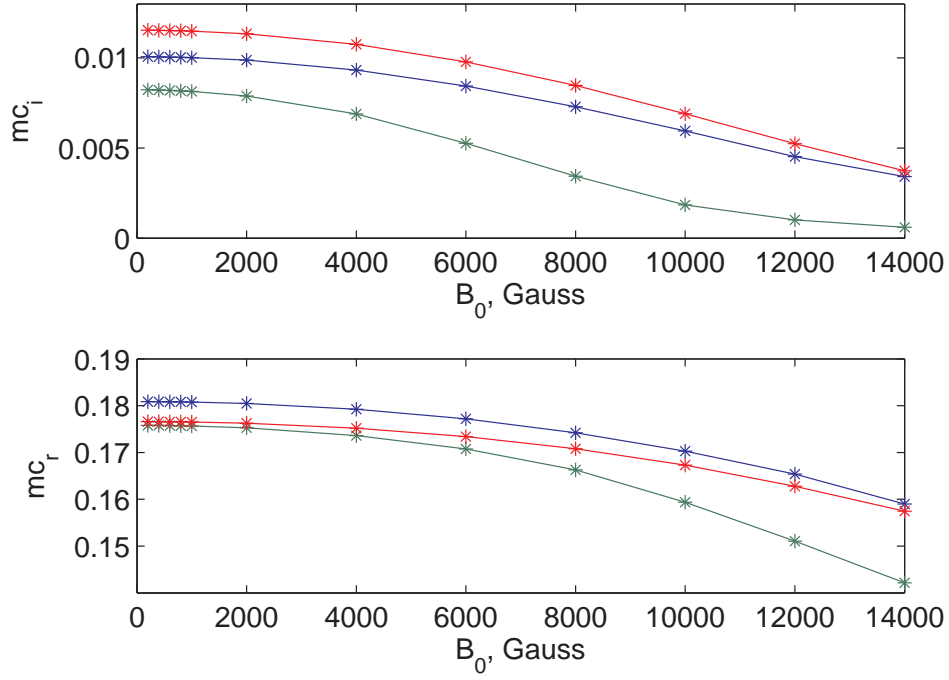


Fig. 4.— Dependence of real (lower panel) and imaginary (upper panel) part of the frequency of the most unstable symmetric harmonic on the magnetic field strength for three different combination of differential rotation parameters. The blue, green and red lines correspond to $(s_2=0.13, s_4=0.1)$, $(s_2=0.11, s_4=0.1)$ and $(s_2=0.11, s_4=0.12)$ respectively.

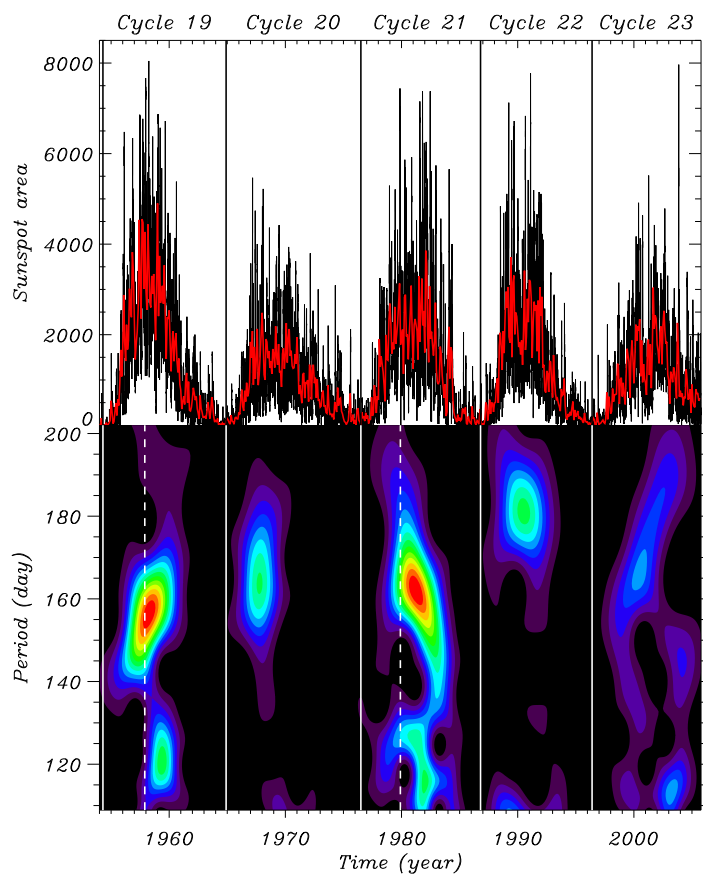


Fig. 5.— Top Panel: Plot of the daily (black) and monthly averaged (red) sunspot areas for solar cycles 19 to 23. Bottom Panel: Time/period diagram calculated using the Morlet wavelet (Torrence & Compo 1998) with $k_0 = 20$. Vertical solid white lines mark the epochs of minimum solar activity, while the two dashed lines correspond to the maximum of cycles 19 and 21. Large power values around 160 days can be seen in cycles 19, 20, 21 and 23, peaking at cycle 19. Power is given in arbitrary units.